Molecular Microbiology (2013) ■ doi:10.1111/mmi.12309

The mobility of two kinase domains in the *Escherichia coli* chemoreceptor array varies with signalling state

Ariane Briegel,[1] Peter Ames,[2] James C. Gumbart,[3] Catherine M. Oikonomou,[4] John S. Parkinson[2] and Grant J. Jensen[1,4]*

[1]*California Institute of Technology, 1200 E. California Blvd, Pasadena, CA 91125, USA.*
[2]*University of Utah, 257 South 1400 East, Salt Lake City, UT 84112, USA.*
[3]*School of Physics, Georgia Institute of Technology, Atlanta, GA 30332, USA.*
[4]*Howard Hughes Medical Institute, 1200 E. California Blvd, Pasadena, CA 91125, USA.*

Summary

Motile bacteria sense their physical and chemical environment through highly cooperative, ordered arrays of chemoreceptors. These signalling complexes phosphorylate a response regulator which in turn governs flagellar motor reversals, driving cells towards favourable environments. The structural changes that translate chemoeffector binding into the appropriate kinase output are not known. Here, we apply high-resolution electron cryotomography to visualize mutant chemoreceptor signalling arrays in well-defined kinase activity states. The arrays were well ordered in all signalling states, with no discernible differences in receptor conformation at 2–3 nm resolution. Differences were observed, however, in a keel-like density that we identify here as CheA kinase domains P1 and P2, the phosphorylation site domain and the binding domain for response regulator target proteins. Mutant receptor arrays with high kinase activities all exhibited small keels and high proteolysis susceptibility, indicative of mobile P1 and P2 domains. In contrast, arrays in kinase-off signalling states exhibited a range of keel sizes. These findings confirm that chemoreceptor arrays do not undergo large structural changes during signalling, and suggest instead that kinase activity is modulated at least in part by changes in the mobility of key domains.

Accepted 24 June, 2013. *For correspondence. E-mail jensen@caltech.edu; Tel. (+1) 626 395 8827; Fax (+1) 626 395 5730.

Introduction

Motile bacteria track gradients of attractant and repellent chemicals with high sensitivity and wide dynamic range using arrays of transmembrane chemoreceptors known as methyl-accepting chemotaxis proteins (MCPs) (Hazelbauer *et al.*, 2008). The external sensing domains of MCP molecules monitor chemoeffector concentrations; their internal signalling domains, comprising extended four-helix coiled-coils, regulate the autophosphorylation activity of an associated kinase, CheA (Fig. 1A). In the extensively studied chemotaxis system of *Escherichia coli*, favourable stimuli, such as an increasing attractant level, downregulate CheA, reducing the flow of phosphoryl groups to the cytoplasmic CheY response regulator, whose phosphorylation status regulates the direction of flagellar motor rotation. High CheA activity elicits clockwise (CW) motor rotation and frequent directional changes; low CheA activity promotes counter-clockwise (CCW) motor rotation and forward swimming. MCPs form trimers of dimers (Kim *et al.*, 1999; Studdert and Parkinson, 2004) that assemble into extended, hexagonally packed arrays (Briegel *et al.*, 2012; Liu *et al.*, 2012). Trimers are linked into the array at their cytoplasmic tips by CheA and the coupling protein CheW (Fig. 1C).

CheA, a homodimer, contains five domains in each subunit (Fig. 1B). During autophosphorylation, the ATP-binding domain (P4) from one subunit transfers a phosphoryl group to a histidine residue in the phosphorylation site domain (P1) of the other subunit (Wolfe and Stewart, 1993; Swanson *et al.*, 1993a). Residues in both P4 and P1 probably play catalytic roles in the phosphorylation reaction (Quezada *et al.*, 2005; Stewart, 2010). The P5 domain at the C-terminus of each subunit binds MCPs (Briegel *et al.*, 2012; Wang *et al.*, 2012) and CheW (Park *et al.*, 2006; Zhao and Parkinson, 2006a,b) to form the ternary signalling complex that couples CheA activity to receptor control (Borkovich *et al.*, 1989). The P2 domain provides a docking site for CheY and CheB (Swanson *et al.*, 1993b), enhancing phosphotransfer efficiency to these response regulator targets of CheA (Stewart *et al.*, 2000) (Fig. 1B). Flanking flexible linkers connect P2 to the P1 domain and to the P3 dimerization domain (Morrison and Parkinson, 1994) (Fig. 1B).

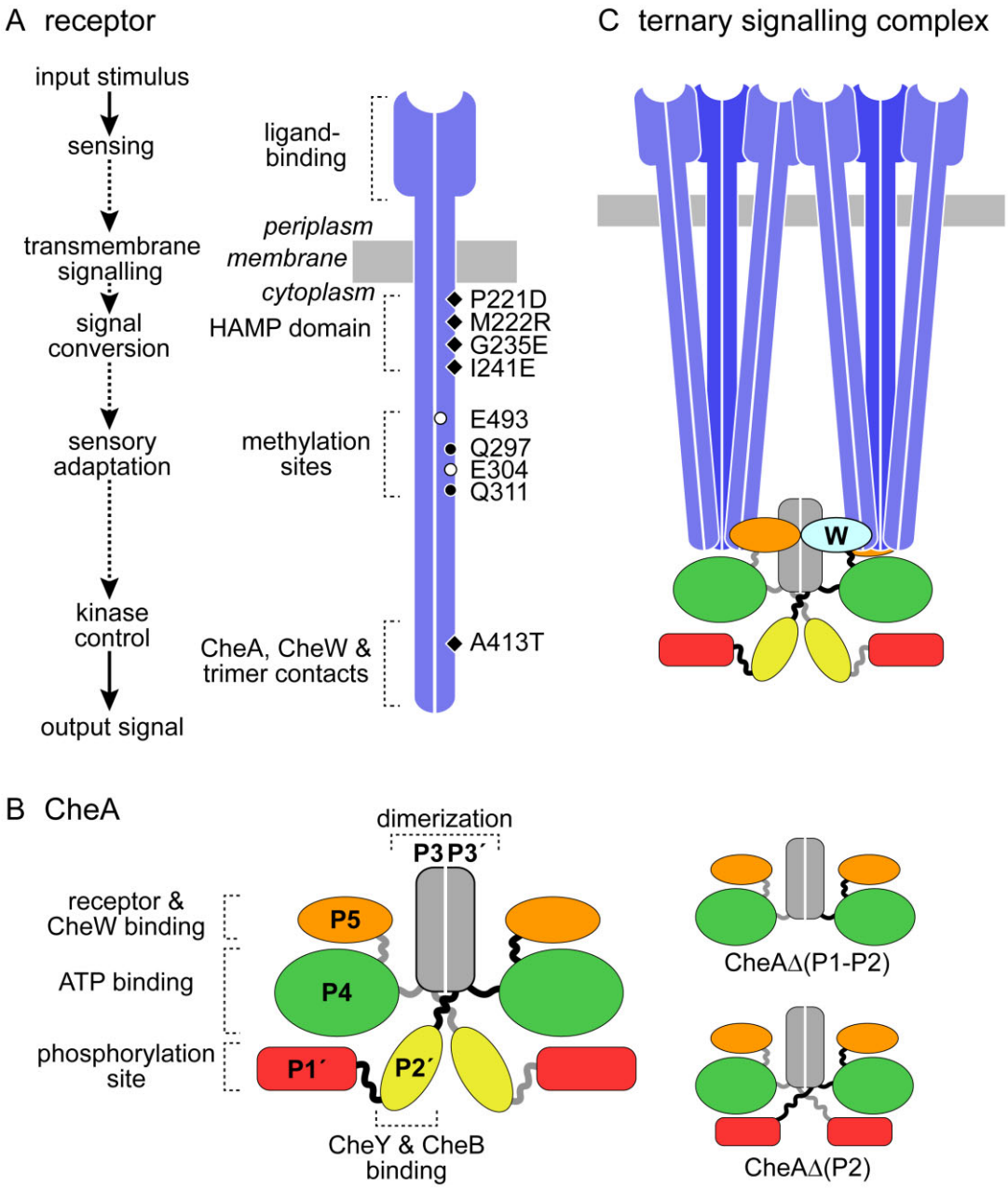

Fig. 1. Structures of MCP receptors, CheA kinase and ternary signalling complexes.
A. Input–output signalling in chemoreceptors of the MCP family. These molecules function as homodimers; the subunits are approximately 500 residues in length and mainly alpha-helical in secondary structure. The approximate positions of amino acid changes used to modify receptor output state in this work are shown.
B. Domain organization of CheA. This autokinase functions as a homodimer. Autophosphorylation is a *trans* reaction, involving interaction of the phosphorylation site domain in one subunit with the ATP-binding domain of the other (Wolfe and Stewart, 1993). Two CheA variants used in the present work are shown at the right.
C. The core signalling units of bacterial chemoreceptors. MCP molecules assemble into trimers of dimers through interactions between their highly conserved cytoplasmic tips (Kim *et al.*, 1999; Studdert and Parkinson, 2004). Two trimers share and control one CheA dimer through binding interactions to its two P5 domains (one is hidden behind the trimer on the right) and to two P5-like CheW coupling proteins (one is hidden behind the trimer on the left). The CheW proteins each interact with a P5 domain, providing additional conformational control connections to the receptors. These core complexes assemble into higher-order arrays through additional P5-CheW interactions (Briegel *et al.*, 2012).

Table 1. Signalling properties of variant Tsr receptors.

			Tsr variant						
Behavioural test	A413T	M222R	EEEE	P221D	QEQE[g]	QQQQ	G235E	I241E	Comments/interpretation
% of flagellar rotation time spent in CW mode in *Δ(cheRB)/(cheRB)*$^+$ strains[a]	0/0	2/0	27/28	0/28	75/27	65/24	91/84	88/80	CW output directly reflects kinase activity level; sensory adaptation system cannot alter output signals of locked receptors
Expression level[b]	1.5	1.1	0.6	1.4	1.0	0.9	1.2	0.9	Variant proteins have normal intracellular stabilities
Receptor clusters and ternary complexes[c]	YES	YES	YES	YES	YES	YES	YES	YES	Normal array and ternary complex formation
Jamming ability[d]	YES	NO	na	YES	na	na	YES	YES	Locked output receptors jam signalling by normal receptors
$K_{1/2}$ [SER][e]	NR	NR	NR	NR	17 μM	200 μM	NR	NR	No response (NR) is due to very low or locked-on kinase activity
Kinase activity[f] SER/KCN	–/0	–/0	–/0	–/0	100/100	84/–	–/80	–/73	
Output state	Locked OFF Kinase activity		Low kinase activity; subject to sensory adaptation control		High kinase activity; subject to stimulus and sensory adaptation control		Locked ON Kinase activity		

a. Tsr expression plasmids were tested in host strains that either carried *(cheRB)*$^+$ or lacked [*Δ(cheRB)*] sensory adaptation functions. The CheR enzyme adds methyl groups to the receptor's adaptation sites; the CheB enzyme demethylates those residues. CheB also deamidates Q residues at the adaptation sites, converting them to E residues that are capable of accepting a methyl group. Receptor methylation augments the activity of CheA kinase molecules coupled to the receptor; demethylation and deamidation reduce the activity of receptor-coupled CheA molecules.
b. Relative to wild-type Tsr (the QEQE form).
c. Approximately 75–85% of cells carrying wild-type Tsr exhibit one or more fluorescent polar spots in these tests (Ames *et al.*, 2002; Mowery *et al.*, 2008). All Tsr variants exhibited similar behaviours.
d. Tsr receptors that have locked signal outputs interfere with Tar signalling, thereby jamming aspartate chemotaxis (Ames *et al.*, 2002). na: not applicable; jamming tests with methylation-state mimics are not meaningful in adaptation-proficient strains.
e. Serine responses of Tsr mutants were assessed with *in vivo* FRET-based kinase assays (Sourjik *et al.*, 2007). $K_{1/2}$ is the serine concentration that produced a 50% reduction in receptor-coupled CheA kinase activity. NR: no serine response detected (up to 10–100 mM serine).
f. Kinase activities (% of wild-type Tsr value) measured by *in vivo* FRET. SER: activity calculated from the FRET change elicited by a saturating serine stimulus; KCN: activity calculated from the FRET change elicited by 3 mM KCN – indicates no kinase value determined by that method.
g. Wild-type Tsr.

Despite a wealth of genetic, biochemical and structural information about the *E. coli* chemotaxis machinery, a central question remains unanswered: how does chemoeffector binding at one end of the MCP molecule toggle the activity of a CheA molecule bound to its other end? One model proposes that kinase activity is controlled by large-scale changes in receptor packing (Lamanna *et al.*, 2005; Borrock *et al.*, 2008; Khursigara *et al.*, 2011; Wu *et al.*, 2011), but no such rearrangements have been seen upon array stimulation in a number of studies (Lybarger and Maddock, 1999; Homma *et al.*, 2004; Liberman *et al.*, 2004; Schulmeister *et al.*, 2008; Erbse and Falke, 2009). An alternative model suggests that CheA inactivation involves sequestration of its P1 phosphotransfer domain (Hamel *et al.*, 2006).

To investigate these models, we used electron cryotomography (ECT) (Gan and Jensen, 2012) to visualize arrays of chemoreceptors mutationally locked in well-defined kinase activity states. We found that the order and packing of the arrays were independent of their activity, implying that signalling does not trigger large-scale reorganization. We did however observe differences in the CheA P1 and P2 densities suggesting that these domains are partially mobile in kinase-active arrays. These findings suggest that receptors control kinase activity at least in part by regulating CheA domain mobility.

Results

Mutant receptors and their kinase activities

To investigate the structural basis for CheA control in receptor signalling complexes, we imaged chemoreceptor arrays in *E. coli* strains containing different forms of the serine receptor, Tsr, as their only MCP (Table S1). We chose Tsr representatives known to form ternary signalling complexes with different kinase activity states (Fig. 1A;

Table 1). The mutations targeted three functionally important regions of Tsr: the HAMP (histidine kinases, adenyl cyclases, MCPs and some phosphatases) domain involved in signal propagation (P221D, M222R, G235E, I241E); the methylation region involved in sensory adaptation (EEEE, QEQE, QQQQ); and the cytoplasmic tip, which binds CheA and CheW (A413T) (Fig. 1A). To prevent confounding effects of sensory adaptation, these Tsr variants were expressed in cells lacking the sensory adaptation enzymes CheR (methyltransferase) and CheB (methylesterase, deamidase). The *cheA* and *cheW* genes were wild-type.

Fluorescence light microscopy confirmed that all of the Tsr variants formed polar arrays (Table 1). Next the kinase activity of each array was quantified in two ways. First, because CheA autophosphorylation is the rate-limiting step in phosphorylation of CheY, and phospho-CheY promotes clockwise (CW) flagellar rotation, we simply counted the percentage of tethered cells rotating clockwise in each strain. Second, because phospho-CheY binds to its phosphatase CheZ, the fluorescence resonance energy transfer (FRET) between CheZ-CFP (FRET donor) and CheY-YFP (FRET acceptor) fusion proteins was monitored (Sourjik *et al*., 2007). The decrease in the FRET signal induced by exposure to a saturating attractant stimulus (defined as inhibiting all receptor-coupled CheA activity) was used as a background-corrected measure of CheA autophosphorylation rate. To measure receptor-coupled kinase activity in cells that could not respond to an attractant stimulus, we blocked ATP production in the cells with KCN, thereby stopping CheA autophosphorylation. The FRET change upon KCN treatment was then used as a measure of cellular CheA activity. Where both FRET-based measurements were possible, the resultant kinase activities were similar. As expected, the results of the flagellar rotation and FRET-based kinase assays agreed well and enabled us to place the mutants into two groups: 'kinase-on' (QEQE, QQQQ, G235E, I241E) and 'kinase-off' (P221D, M222R, EEEE, A413T) (Table 1, Fig. S1).

Receptor arrays in all signalling states are well ordered

ECT of cells of each strain revealed that all eight of the mutant receptors formed well-ordered, extended arrays (Fig. 2). Some fragmentation of arrays into two or a few large patches was occasionally observed (Fig. S2), but because such fragmentation occurred in all mutant and wild-type strains, both in this study and in previous studies (Briegel *et al*., 2009), it was likely a result of cell lysis and flattening rather than signalling state. The array order and spacing (12 nm) of all mutant arrays were indistinguishable from one another and from previously reported chemoreceptor arrays (Fig. 2).

The size of a keel-like density varies in different receptor signalling states

As before (Briegel *et al*., 2012), subtomogram averages corrected for the contrast transfer function (CTF) revealed a 'two-on-two' organization of the receptor trimers-of-dimers in which pairs of dimers faced each other at each interface around the ring (Fig. 3). Although signal-related structural changes were not detected in the receptors themselves, keel-like densities of varying size were observed just below the receptor tips (i.e. closer to the cell centre) (Fig. 3). Top views revealed that the keels connected opposing trimers, but on only three sides of each hexagon (Fig. 3 arrowheads), alternating with gaps (Fig. 3 asterisks).

To compare the volume of the keel densities in different mutants, we first aligned the subtomogram averages by fitting a crystal structure of a Tsr receptor tip into each average with molecular dynamics flexible fitting (MDFF). We then selected a reasonable density threshold for each average that just enclosed at least one of the three receptor dimers. Because the averages were not identical in quality or resolution, to reduce errors introduced by the choice of different thresholds, we calculated the keel volume as a percentage of the total volume of two trimers of receptor dimers and their associated keel. The keel volumes of the kinase-active mutants fell between 13% and 18%. In contrast, kinase inactive mutants exhibited widely varying keel volumes. Two (A413T and EEEE) had large keel densities (30% and 24% respectively), one was similar to the kinase active mutants (P221D, 18%), and one had the smallest keel density (M222R, 6%).

The keel density comprises the P1 and P2 domains of CheA

The position of the keel density matched that of CheA dimers in the array (Briegel *et al*., 2012; Liu *et al*., 2012), suggesting that it might correspond to one or more CheA domains. Liu *et al*. observed a similar structure in arrays of wild-type receptors and suggested that it represented P1 (Liu *et al*., 2012). We found that the keel comprises at least two CheA domains, P1 and P2 (Fig. 4). In a strain containing locked-off A413T receptors and CheA molecules that lacked both the P1 and P2 domains (see Fig. 1B), the keel density was completely missing (Fig. 4A–C; blue density). Images of CheAΔ(P1–P2) in arrays of a different kinase-off receptor mutant (P221D) produced an identical result (Fig. 4G–I; cyan density). Previous characterization of this CheA mutant showed that it was still capable of forming ternary signalling complexes and, when supplied with P1 domains *in trans*, its phosphorylation activity still responded to stimulus control (Garzon and Parkinson, 1996). Because free P1 domains are not known to bind

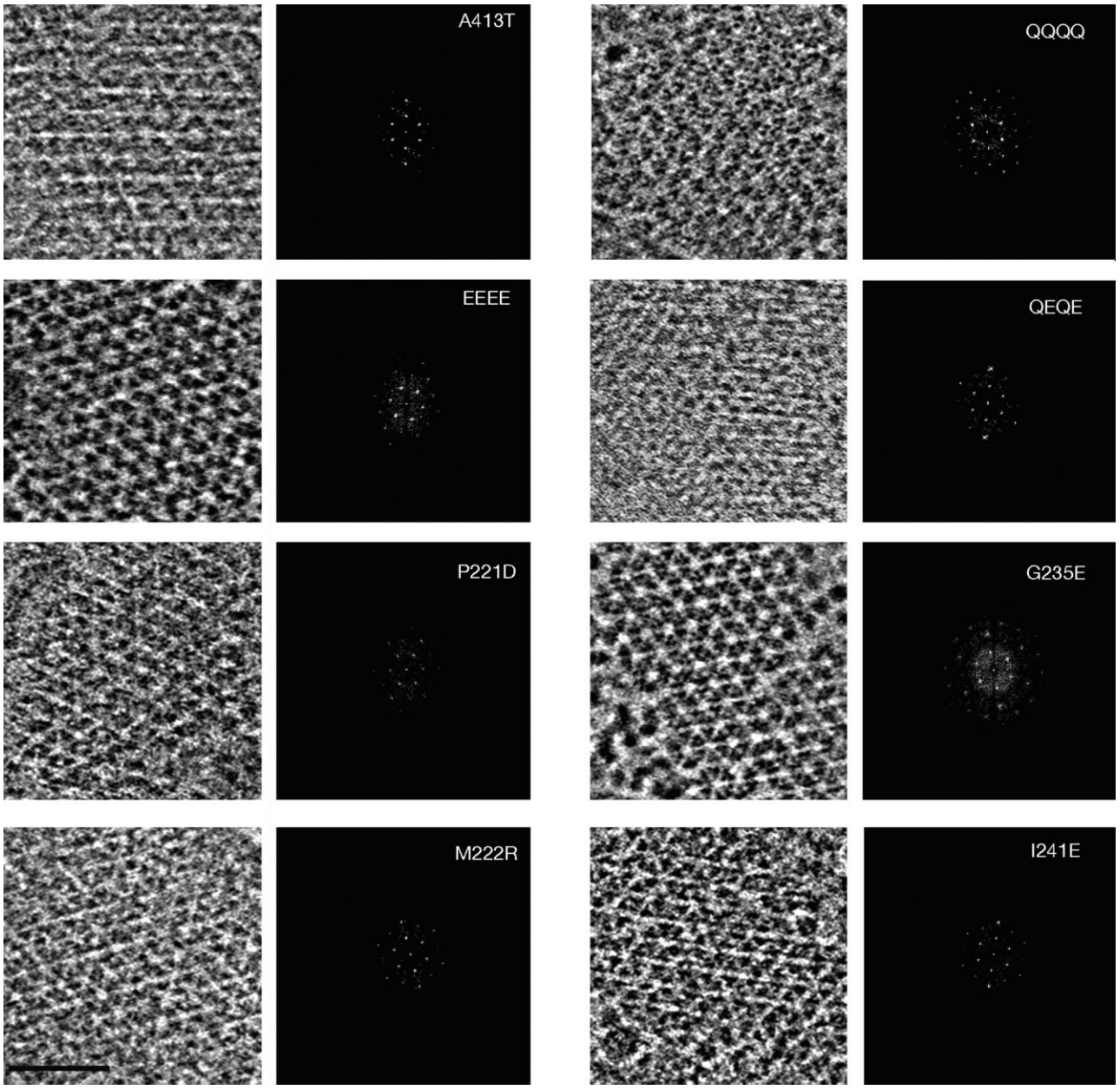

Fig. 2. No large-scale differences are evident in mutant receptor arrays. Representative tomographic slices and corresponding power spectra of kinase-inactive (left column) and kinase-active receptor mutant arrays (right column). All arrays have comparable hexagonal organization with 12 nm spacing. Scale bar (bottom left panel): 30 nm.

directly to receptors, this implies that receptor signalling must involve conformational changes in the P3–P4–P5 domains of CheA. In a strain with the A413T mutant receptor and CheA molecules lacking only the P2 domain, the keel was partially missing (Fig. 4D–F; blue density). The residual keel formed a clamp-like density (arrows in Fig. 4D–F) surrounding an empty centre region. The P2-deleted CheA molecule is also known to form ternary signalling complexes and to respond to stimuli (Jahreis *et al.*, 2004). Thus the partial keel formed by the CheAΔP2 molecule most likely corresponds to the P1 domain, possibly docked to its interaction partner, the ATP-binding P4 domain.

Sequestered CheA molecules resist proteolysis

Because densities in subtomogram averages depend on the consistent localization of array components, we hypothesized that the size of the keels might reflect the mobility of CheA domains P1 and P2. To test this idea, we

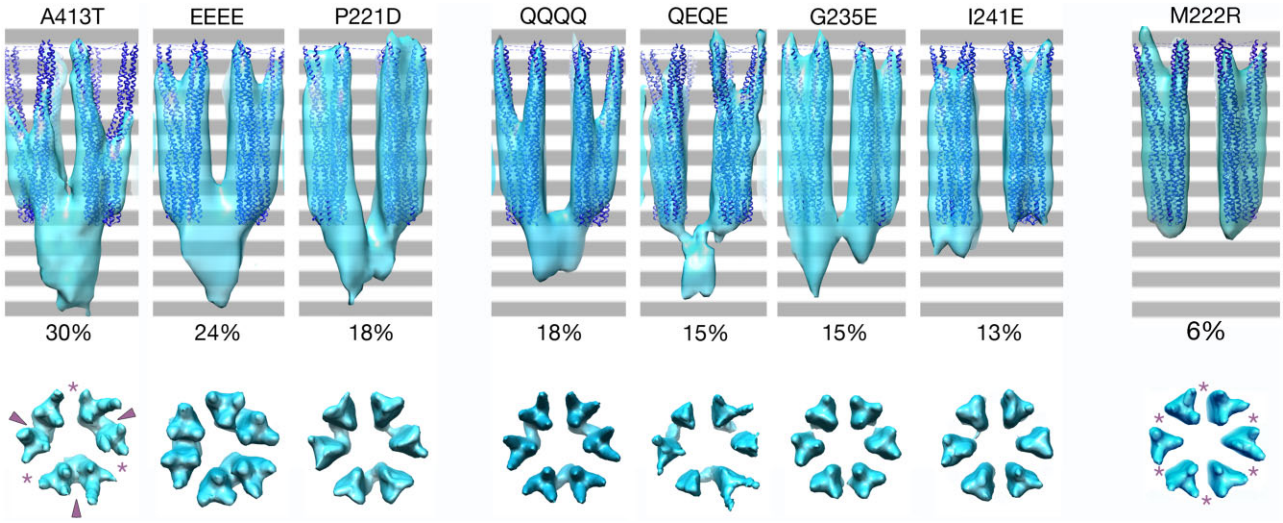

Fig. 3. Keel electron density varies in ternary signalling complexes in different output states. Image averages are shown for signalling complexes of eight Tsr variants with the amino acid changes listed across the top: wild-type receptor subunits (QEQE) have Q residues at two of the four methylation sites; the EEEE and QQQQ variants mimic the fully unmethylated or fully methylated forms of the receptor. The A413T, P221D, M222R, G235E and I241E mutant receptors are variants of the QEQE wild-type. Receptor crystal structures (purple) were fitted into subtomogram averages by MDFF for reference and alignment. An extra keel-like density, most prominent in the A413T complexes, is seen below the receptors in the side views (top row). The numbers below the keels give the volume of the keel density as a percentage of the total volume occupied by two trimers plus the keel at an appropriate threshold (shown in blue). Bottom row: top views showing keel densities connecting adjacent trimers (arrowheads), alternating with gaps around the hexagons (asterisks).

looked for differences in protease sensitivity of CheA molecules in the mutant receptor arrays. In CheA molecules that are not associated with receptors in signalling complexes, the flexible linkers flanking the P2 domain are preferred targets of proteolysis (Morrison and Parkinson, 1994). Accordingly, we exposed arrays in gently lysed cells to proteinase K briefly and then analysed the CheA degradation products by Western blot. The antibody used recognizes epitopes primarily in P1 and therefore detects cleavage events that separate this domain from intact CheA. We found that CheA was more rapidly cleaved in strains with small keel volumes than in strains with large keel volumes (Fig. 5), consistent with increased mobility of P1 and P2.

Discussion

Whether or not a chemotactic stimulus alters the gross structure of the chemoreceptor array has been a contentious topic in the chemotaxis literature. While some studies have found signalling-dependent changes in receptor packing (Lamanna *et al.*, 2005; Borrock *et al.*, 2008; Khursigara *et al.*, 2011; Wu *et al.*, 2011), others have not (Lybarger and Maddock, 1999; Homma *et al.*, 2004; Liberman *et al.*, 2004; Schulmeister *et al.*, 2008; Erbse and Falke, 2009). In the present study, ECT images showed that eight *E. coli* strains with widely variant kinase activity all contained well-ordered, hexagonally packed chemoreceptor arrays with identical 12 nm lattice spacing. This confirms the findings of a previous ECT study of *Caulobacter crescentus* before and after exposure to attractant (Briegel *et al.*, 2011). We conclude that receptor arrays do not undergo large rearrangements between signalling states. We did, however, find that CheA domains P1 and P2 were more mobile in kinase-active arrays than in arrays containing the A413T and EEEE receptors, which are locked in a kinase-off state. Although we cannot be certain that Tsr-A413T is locked in a physiologically relevant signalling state, the unmethylated EEEE form of Tsr is a component of native signalling complexes in adaptation-proficient strains. Because removal of methyl groups drives receptors towards the attractant-induced kinase-off state, the EEEE form most likely represents this physiologically relevant signalling state (Hazelbauer *et al.*, 2008).

Sequestration of the P1 domain was previously proposed as a mechanism that prevents productive interactions with P4 (Hamel *et al.*, 2006), but the data presented here are the first direct evidence for such a model. We suggest that stimulus inputs promote structural changes along the length of the receptors, which in turn impart conformational changes to CheA through receptor-P5 and receptor-CheW-P5 connections (Fig. 1C). Changes in the conformation or orientation of the ATP-binding CheA-P4 domain then modulate its interaction with the CheA-P1 phosphorylation site domain. We further propose that in the kinase-on signalling state, increased mobility of the P1 and P2 domains allows for cycles of P1 engagement, phosphorylation and release. Trapping the P1 and P2 domains in a

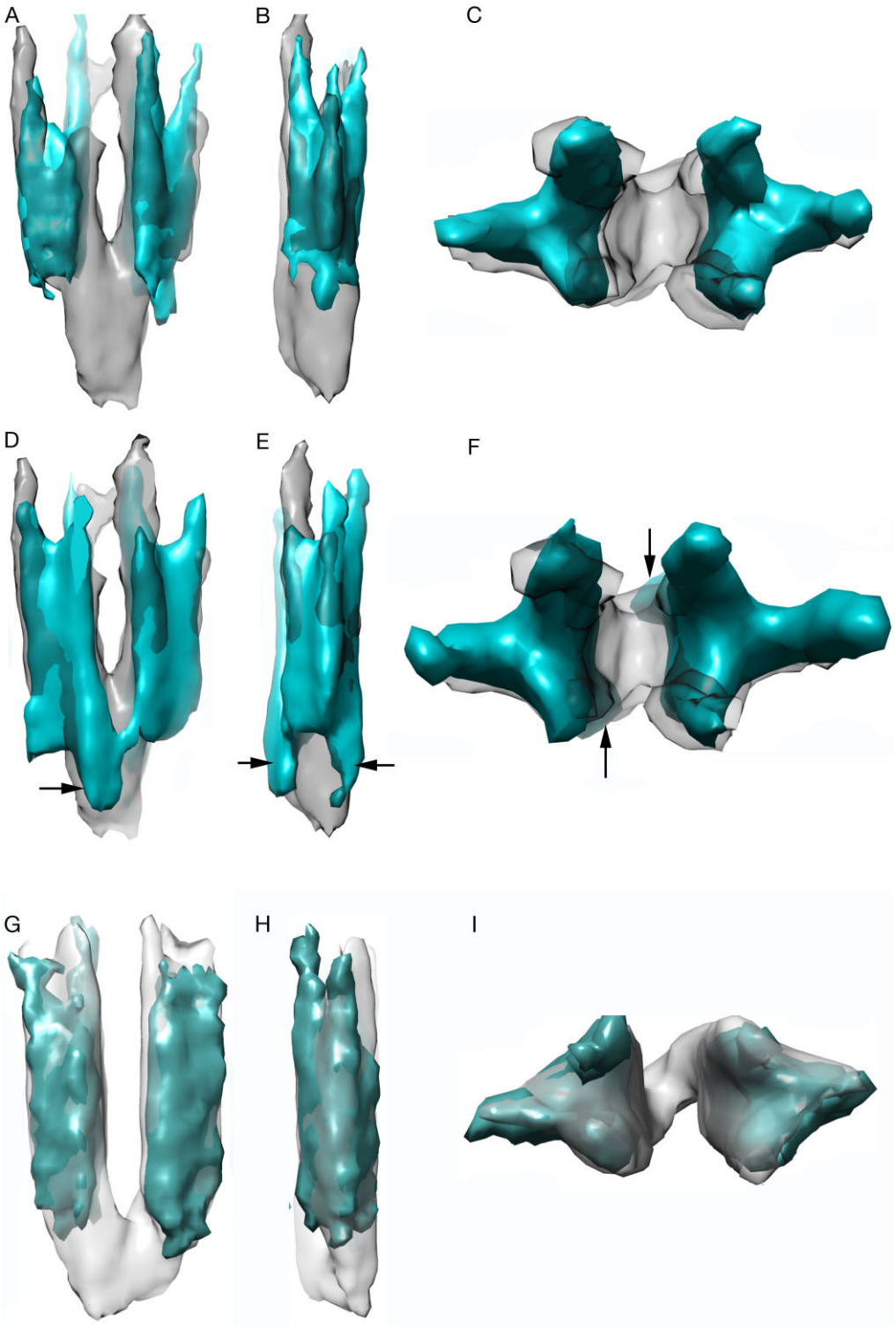

Fig. 4. Keel electron density comprises CheA subunits P1 and P2. From left to right: side views, side views rotated 90°, top views.
A–F. Signalling complexes of the A413T receptor that compare the keels seen with wild-type CheA (grey) to those seen with CheA mutants (blue).
A–C. Wild-type CheA and CheAΔ(P1–P2) signalling complexes.
D–F. Wild-type CheA and CheAΔP2 signalling complexes. Black arrows point to clamp-like structures on each side of the keel that probably contain the P1 domain and possibly part of the P4 domain with which it interacts.
G–I. Signalling complexes of the P221D receptor that compare the keels seen with wild-type CheA (light grey) to those seen with CheAΔ(P1–P2) (cyan).

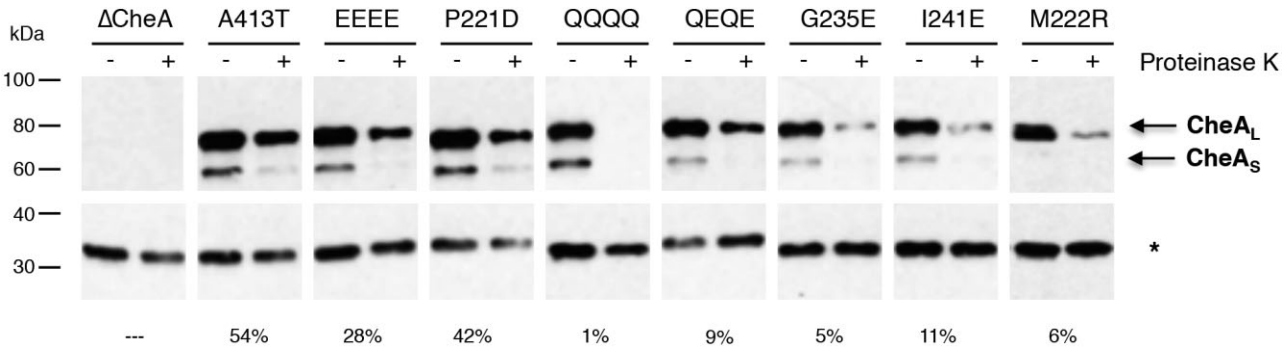

Fig. 5. CheA protease sensitivity corresponds to keel size. Western blots of mutant strains without (–) or with (+) treatment with proteinase K. Top: α-CheA. Arrows indicate long and short isoforms of CheA. Bottom: loading control (proteinase K-resistant background band (*) detected by α-β-lactamase). Values at bottom indicate per cent of CheA$_L$ signal remaining after treatment for each strain.

static, non-productive complex with P4 (manifest here as a large keel density with low susceptibility to proteolysis) appears to be one way to deactivate the kinase.

Although we were unable to resolve conformational differences along the receptors themselves, the idea that the kinase is controlled by changes in the mobility of its domains supports an important principle of the dynamic-bundle (Zhou *et al*., 2009) and yin-yang (Swain *et al*., 2009) models of receptor signalling. The dynamic-bundle model asserts that the packing stabilities of the HAMP bundle and the neighbouring methylation bundle are in opposition: structural changes (induced by stimuli, adaptational modifications or amino acid replacements) that destabilize one element will stabilize the other. The yin-yang model postulates a similar opposing stability interaction between the methylation bundle and the receptor tip. Here we have shown that at least the downstream target of these signals, CheA, does in fact have states with different dynamic properties.

Previous work has suggested, however, that there are more than just two simple 'kinase-on' and 'kinase-off' states. Instead, both HAMP-stabilizing and HAMP-destabilizing lesions were found to deactivate the kinase, leading to a biphasic output model in which intermediate HAMP stabilities result in kinase activation, whereas stability perturbations to either extreme result in deactivation (Zhou *et al*., 2011). Our observations echo these ideas, because the mutant arrays with intermediate keel sizes had active kinases, whereas arrays with both the largest (A413T and EEEE) and smallest (M222R) keels were kinase-off. The M222R lesion in particular was previously suggested to drive receptor output to a kinase-off state [CCW(B)] that differs from the physiologically relevant, attractant-induced kinase-off state [CCW(A)] (Zhou *et al*., 2011). We assume that in the M222R receptor complex additional conformational changes in P4 or other components block CheA activity despite its mobile P1 and P2 domains. The P221D mutant is more difficult to interpret, because it exhibited an intermediate P1–P2 dynamic state but was still kinase-off. Conceivably, as with M222R, structural changes other than P1 and P2 immobilization can block kinase activity. Further imaging of additional mutant receptors and signalling complexes, and to higher resolution, should clarify these issues.

Experimental procedures

Bacterial strains

Strains used in this study (Table S1) were isogenic derivatives of RP437, a wild-type chemotaxis derivative of *E. coli* K-12 (Parkinson and Houts, 1982). Mutant alleles of *tsr* and *cheA* were crossed from PCR-amplified DNA fragments into the corresponding *E. coli* chromosomal loci by λ Red-mediated homologous recombination as described (Ames *et al*., 2008). Genotypes were verified by sequencing PCR-amplified chromosomal DNA.

Plasmids

Regulatable Tsr expression plasmids [pRR53 (Studdert and Parkinson, 2005); pPA114 (Ames *et al*., 2002)] were used to characterize signalling properties of mutant receptor alleles in the tests described below. For *in vivo* kinase assays, FRET reporters were expressed from regulated plasmids that were compatible with the mutant Tsr plasmids: pVS88 (Sourjik *et al*., 2007) (compatible with pPA114) and pRZ30 (this work, compatible with pRR53).

Flagellar rotation assays

Strains containing Tsr expression plasmids were grown to mid-exponential phase in tryptone broth (TB) at 30°C and tethered to microscope coverslips with anti-flagellum antibodies to measure clockwise (CW) flagellar rotation time (Ames *et al*., 2002; Zhou *et al*., 2011).

Receptor expression levels

The intracellular levels of the variant Tsr proteins expressed from regulatable plasmids were measured as described

(Ames and Parkinson, 2006). The inducer concentrations used produced an expression level of wild-type Tsr comparable to that of chromosomally encoded Tsr in plasmid-free cells. Cell lysates were subjected to denaturing gel electrophoresis and Tsr molecules detected by Western blotting with a rabbit polyclonal antiserum directed against the highly conserved protein interaction region of the Tsr molecule.

Cluster and ternary complex formation assays

The ability of variant receptors to form macroscopic clusters, characteristic of receptor arrays, was determined by fluorescence microscopy, as described (Ames *et al*., 2002; Mowery *et al*., 2008). Direct tests of clustering ability used a YFP-CheR reporter, which binds directly to the C-terminus of Tsr molecules (Wu *et al*., 1996). Ternary complex formation was assessed in a similar manner with a YFP-CheZ reporter, which binds to $CheA_S$ molecules that lack the P1 domain (Cantwell *et al*., 2003).

Jamming assays

Tsr plasmids were expressed in a strain that was wild-type for aspartate chemotaxis and tested for ability to block or jam Tar receptor function, as described (Ames *et al*., 2002).

In vivo *FRET kinase assays*

Sensitivity of mutant Tsr receptors to a serine stimulus was assessed with *in vivo* FRET-based kinase assays (Sourjik *et al*., 2007). Plasmids expressing Tsr variants were tested in strain UU2567 that also carried a compatible plasmid expressing the CheY-YFP and CheZ-CFP FRET reporters.

Electron cryotomography

Escherichia coli strains were grown to mid-exponential phase at 30°C in TB. Cells were concentrated and incubated with 0.3 μg ml^{-1} penicillin for 1 h at 30°C with shaking. Lysed cells were kept on ice until freezing. Immediately before plunge freezing, the cell lysates were mixed with colloidal gold pretreated with BSA to avoid particle aggregation (Iancu *et al*., 2007).

Three microlitres of gold-lysate mixture were applied to R2/2 copper/rhodium Quantifoil™ grids (Quantifoil Micro Tools), or R2/2 C-flat™ grids (Protochips). Excess liquid was blotted and the grids were plunge frozen in liquid ethane or ethane propane mixture (Iancu *et al*., 2007; Tivol *et al*., 2008).

Images were collected using an FEI Polara™ (FEI) 300 kV field emission gun transmission electron microscope equipped with a Gatan energy filter and a lens-coupled 4000 × 4000 Ultracam (Gatan) or a direct detector in counting mode using the 'K2 Summit' detector (Gatan). Tilt series from −65° to 65° in 1 degree increments and an underfocus of −8 to −10 μm, and effective pixel sizes after 2 × 2 binning between 6.4 and 6.6 Å were recorded using Leginon or UCSFtomo (Zheng *et al*., 2007; Suloway *et al*., 2009). A cumulative dose of ~ 160 electrons/$Å^2$ was used for each tilt series. Tilt series were aligned using the IMOD software package (Kremer *et al*., 1996), CTF corrected (Kremer *et al*., 1996; Fernandez *et al*., 2006), and SIRT reconstructed using TOMO3D (Agulleiro and Fernandez, 2011). Subvolume averaging and threefold symmetrizing was done using PEET (Nicastro *et al*., 2006). Visualization and volume measurements were done using Chimera software (Pettersen *et al*., 2004).

Molecular dynamics flexible fitting (MDFF)

As a starting point for modelling a hexamer of trimeric receptors, a previously constructed model of the Tsr receptor up to the level of the HAMP domain was used (Briegel *et al*., 2012). MDFF, a method that permits one to flexibly fit atomic structures in lower resolution density maps while preserving the structures' stereochemical accuracy (Trabuco *et al*., 2008), was then used on each map to generate unique fitted structures in full atomistic detail. The fitting simulations were carried out with the molecular dynamics program NAMD 2.9 (Phillips *et al*., 2005). Restraints were applied to maintain the proteins' secondary structure and chirality, as well as to prevent the formation of *cis* peptide bonds (Schreiner *et al*., 2011). Additional restraints to limit distortions of tertiary structure in the individual trimers and to enforce hexagonal symmetry between the distinct trimers were also utilized (Chan *et al*., 2011). Fitting was carried out in multiple stages over 1.5 ns for each map in order to optimize the position of the hexamer in the density and then the fit of the trimers themselves.

CheA proteolysis in receptor arrays

Escherichia coli strains were grown to mid-exponential phase in TB at 30°C with shaking. Cells were lysed by incubation with 0.3 μg ml^{-1} penicillin for 1 h at 30°C with shaking and collected by centrifugation. Lysates were divided into two sets; one set was untreated and the other was exposed to 10 μg ml^{-1} Proteinase K for 30 min at 37°C. Proteinase K was then inactivated by addition of 5 mM phenylmethylsulphonyl fluoride; after 2 min, Laemmli sample buffer (Laemmli, 1970) was added and samples were boiled for 10 min and analysed by Western blotting. CheA-derived bands were visualized with polyclonal rabbit anti-CheA serum (1:1500) and donkey anti-rabbit-horseradish peroxidase (HRP) secondary antibody (1:60 000; Pierce). To correct for loading differences, normalization was carried out using an unknown protease-insensitive protein detected by β-lactamase antiserum (1:2000).

Accession numbers

The EMDB accession numbers for the subvolume averages reported in this article are as follows (strains in parentheses): EMD-5541 (A413T), EMD-5542 (P221D), EMD-5543 (EEEE), EMD-5545 (QQQQ), EMD-5546 (I241E), EMD-5547 (G235E), EMD-5548 (QEQE), EMD-2414 (M222R), EMD-5549 (A413TΔP1P2), EMD-5550 (A413TΔP2), EMD-5716 (P221DΔP1P2).

Acknowledgements

This work was supported in part by NIGMS Grants GM101425 (to G.J.J. and J.C.G.) and GM19559 (to J.S.P.),

as well as a gift to Caltech from the Gordon and Betty Moore Foundation. The Protein-DNA Core Facility at the University of Utah receives support from National Cancer Institute Grant CA42014 to the Huntsman Cancer Institute.

References

Agulleiro, J.I., and Fernandez, J.J. (2011) Fast tomographic reconstruction on multicore computers. *Bioinformatics* **27:** 582–583.

Ames, P., and Parkinson, J.S. (2006) Conformational suppression of inter-receptor signaling defects. *Proc Natl Acad Sci USA* **102:** 9292–9297.

Ames, P., Studdert, C.A., Reiser, R.H., and Parkinson, J.S. (2002) Collaborative signaling by mixed chemoreceptor teams in *Escherichia coli*. *Proc Natl Acad Sci USA* **99:** 7060–7065.

Ames, P., Zhou, Q., and Parkinson, J.S. (2008) Mutational analysis of the connector segment in the HAMP domain of Tsr, the *Escherichia coli* serine chemoreceptor. *J Bacteriol* **190:** 6676–6685.

Borkovich, K.A., Kaplan, N., Hess, J.F., and Simon, M.I. (1989) Transmembrane signal transduction in bacterial chemotaxis involves ligand-dependent activation of phosphate group transfer. *Proc Natl Acad Sci USA* **86:** 1208–1212.

Borrock, M.J., Kolonko, E.M., and Kiessling, L.L. (2008) Chemical probes of bacterial signal transduction reveal that repellents stabilize and attractants destabilize the chemoreceptor array. *ASC Chem Biol* **3:** 101–109.

Briegel, A., Ortega, D.R., Tocheva, E.I., Wuichet, K., Li, Z., Chen, S., *et al*. (2009) Universal architecture of bacterial chemoreceptor arrays. *Proc Natl Acad Sci USA* **106:** 17181–17186.

Briegel, A., Beeby, M., Thanbichler, M., and Jensen, G.J. (2011) Activated chemoreceptor arrays remain intact and hexagonally packed. *Mol Microbiol* **82:** 748–757.

Briegel, A., Li, X., Bilwes, A.M., Hughes, K.T., Jensen, G.J., and Crane, B.R. (2012) Bacterial chemoreceptor arrays are hexagonally packed trimers of receptor dimers networked by rings of kinase and coupling proteins. *Proc Natl Acad Sci USA* **109:** 3766–3771.

Cantwell, B.J., Draheim, R.R., Weart, R.B., Nguyen, C., Stewart, R.C., and Manson, M.D. (2003) CheZ phosphatase localizes to chemoreceptor patches via CheA-short. *J Bacteriol* **185:** 2354–2361.

Chan, K.-Y., Gumbart, J., McGreevy, R., Watermeyer, J.M., Sewell, B.T., and Schulten, K. (2011) Symmetry-restrained flexible fitting for symmetric EM maps. *Structure* **19:** 1211–1218.

Erbse, A.H., and Falke, J.J. (2009) The core signaling proteins of bacterial chemotaxis assemble to form an ultrastable complex. *Biochemistry* **48:** 6975–6987.

Fernandez, J.J., Li, S., and Crowther, R.A. (2006) CTF determination and correction in electron cryotomography. *Ultramicroscopy* **106:** 587–596.

Gan, L., and Jensen, G.J. (2012) Electron tomography of cells. *Q Rev Biophys* **45:** 27–56.

Garzon, A., and Parkinson, J.S. (1996) Chemotactic signaling by the P1 phosphorylation domain liberated from the CheA histidine kinase of *Escherichia coli*. *J Bacteriol* **178:** 6752–6758.

Hamel, D.J., Zhou, H., Starich, M.R., Byrd, R.A., and Dahlquist, F.W. (2006) Chemical-shift-perturbation mapping of the phosphotransfer and catalytic domain interaction in the histidine autokinase CheA from *Thermotoga maritima*. *Biochemistry* **45:** 9509–9517.

Hazelbauer, G.L., Falke, J.J., and Parkinson, J.S. (2008) Bacterial chemoreceptors: high-performance signaling in networked arrays. *Trends Biochem Sci* **33:** 9–19.

Homma, M., Shiomi, D., Homma, M., and Kawagishi, I. (2004) Attractant binding alters arrangement of chemoreceptor dimers within its cluster at the cell pole. *Proc Natl Acad Sci USA* **101:** 3462–3467.

Iancu, C.V., Tivol, W.F., Schooler, J.B., Dias, D.P., Henderson, G.P., Murphy, G.E., *et al*. (2007) Electron cryotomography sample preparation using the Vitrobot. *Nat Protoc* **1:** 2813–2819.

Jahreis, K., Morrison, T.B., Garzon, A., and Parkinson, J.S. (2004) Chemotactic signaling by an *Escherichia coli* CheA mutant that lacks the binding domain for phosphoacceptor partners. *J Bacteriol* **186:** 2664–2672.

Khursigara, C.M., Lan, G., Neumann, S., Wu, X., Ravindran, S., Borgia, M.J., *et al*. (2011) Lateral density of receptor arrays in the membrane plane influences sensitivity of the *E. coli* chemotaxis response. *EMBO J* **30:** 1719–1729.

Kim, K.K., Yokota, H., and Kim, S.H. (1999) Four-helical-bundle structure of the cytoplasmic domain of a serine chemotaxis receptor. *Nature* **400:** 787–792.

Kremer, J.R., Mastronarde, D.N., and McIntosh, J.R. (1996) Computer visualization of three-dimensional data using Imod. *J Struct Biol* **116:** 71–76.

Laemmli, U.K. (1970) Cleavage of structural proteins during the assembly of the head of bacteriophage T4. *Nature* **227:** 680–685.

Lamanna, A.C., Ordal, G.W., and Kiessling, L.L. (2005) Large increases in attractant concentration disrupt the polar localization of bacterial chemoreceptors. *Mol Microbiol* **57:** 774–785.

Liberman, L., Berg, H.C., and Sourjik, V. (2004) Effect of chemoreceptor modification on assembly and activity of the receptor-kinase complex in *Escherichia coli*. *J Bacteriol* **186:** 6643–6646.

Liu, J., Hu, B., Morado, D.R., Jani, S., Manson, M.D., and Margolin, W. (2012) Molecular architecture of chemoreceptor arrays revealed by cryoelectron tomography of *Escherichia coli* minicells. *Proc Natl Acad Sci USA* **109:** E1481–E1488.

Lybarger, S.R., and Maddock, J.R. (1999) Clustering of the chemoreceptor complex in *Escherichia coli* is independent of the methyltransferase CheR and the methylesterase CheB. *J Bacteriol* **181:** 5527–5529.

Morrison, T.B., and Parkinson, J.S. (1994) Liberation of an interaction domain from the phosphotransfer region of CheA, a signaling kinase of *E. coli*. *Proc Natl Acad Sci USA* **91:** 5485–5489.

Mowery, P., Ostler, J.B., and Parkinson, J.S. (2008) Different signaling roles of two conserved residues in the cytoplasmic hairpin tip of Tsr, the *E. coli* serine chemoreceptor. *J Bacteriol* **190:** 8065–8074.

Nicastro, D., Schwartz, C.L., Pierson, J., Gaudette, R., Porter, M.E., and McIntosh, J.R. (2006) The molecular architecture of axonemes revealed by cryoelectron tomography. *Science* **313:** 944–948.

Park, S.-Y., Borbat, P.P., Gonzalez-Bonet, G., Bhatnagar, J., Pollard, A.M., Freed, J.H., *et al.* (2006) Reconstruction of the chemotaxis receptor-kinase assembly. *Nat Struct Mol Biol* **13:** 400–407.

Parkinson, J.S., and Houts, S.E. (1982) Isolation and behavior of *Escherichia coli* deletion mutants lacking chemotaxis functions. *J Bacteriol* **151:** 106–113.

Pettersen, E.F., Goddard, T.D., Huang, C.C., Couch, G.S., Greenblatt, D.M., Meng, E.C., and Ferrin, T.E. (2004) UCSF Chimera – a visualization system for exploratory research analysis. *J Comput Chem* **25:** 1605–1612.

Phillips, J.C., Braun, R., Wang, W., Gumbart, J., Tajkhorshid, E., Villa, E., *et al.* (2005) Scalable molecular dynamics with NAMD. *J Comput Chem* **26:** 1781–1802.

Quezada, C.M., Hamel, D.J., Gradinaru, C., Bilwes, A.M., Dahlquist, F.W., Crane, B.R., and Simon, M.I. (2005) Structural and chemical requirements for histidine phosphorylation by the chemotaxis kinase CheA. *J Biol Chem* **280:** 30581–30585.

Schreiner, E., Trabuco, L.G., Freddolino, P.L., and Schulten, K. (2011) Stereochemical errors and their implications for molecular dynamics simulations. *BMC Bioinformatics* **12:** 190.

Schulmeister, S., Ruttorf, M., Thiem, S., Kentner, D., Lebiedz, D., and Sourjik, V. (2008) Protein exchange dynamics at chemoreceptor clusters in *E. coli*. *Proc Natl Acad Sci USA* **105:** 6403–6408.

Sourjik, V., Vaknin, A., Shimizu, T.S., and Berg, H.C. (2007) *In vivo* measurement by FRET of pathway activity in bacterial chemotaxis. *Methods Enzymol* **423:** 365–391.

Stewart, R.C. (2010) Protein histidine kinases: assembly of active sites and their regulation in signaling pathways. *Curr Opin Microbiol* **13:** 133–141.

Stewart, R.C., Jahreis, K., and Parkinson, J.S. (2000) Rapid phosphotransfer to CheY from a CheA protein lacking the CheY-binding domain. *Biochemistry* **39:** 13157–13165.

Studdert, C.A., and Parkinson, J.S. (2004) Crosslinking snapshots of bacterial chemoreceptor squads. *Proc Natl Acad Sci USA* **101:** 2117–2122.

Studdert, C.A., and Parkinson, J.S. (2005) Insights into the organization and dynamics of bacterial chemoreceptor clusters through *in vivo* crosslinking studies. *Proc Natl Acad Sci USA* **102:** 15623–15628.

Suloway, C., Shi, J., Cheng, A., Pulokas, J., Carragher, B., Potter, C.S., *et al.* (2009) Fully automated, sequential tilt-series acquisition with Leginon. *J Struct Biol* **167:** 11–18.

Swain, K.E., Gonzalez, M.A., and Falke, J.J. (2009) Engineered socket study of signaling through a four-helix bundle: evidence for a yin-yang mechanism in the kinase control module of the aspartate receptor. *Biochemistry* **48:** 9266–9277.

Swanson, R.V., Bourret, R.B., and Simon, M.I. (1993a) Intermolecular complementation of the kinase activity of CheA. *Mol Microbiol* **8:** 435–441.

Swanson, R.V., Schuster, S.C., and Simon, M.I. (1993b) Expression of CheA fragments which define domains encoding kinase, phosphotransfer, and CheY binding activities. *Biochemistry* **32:** 7623–7629.

Tivol, W., Briegel, A., and Jensen, G.J. (2008) An Improved cryogen for plunge freezing. *Microsc Microanal* **14:** 375–379.

Trabuco, L.G., Villa, E., Mitra, K., Frank, J., and Schulten, K. (2008) Flexible fitting of atomic structures into electron microscopy maps using molecular dynamics. *Structure* **16:** 673–683.

Wang, X., Vu, A., Lee, K., and Dahlquist, F.W. (2012) CheA-receptor interaction sites in bacterial chemotaxis. *J Mol Biol* **422:** 282–290.

Wolfe, A.J., and Stewart, R.C. (1993) The short form of the CheA protein restores kinase activity and chemotactic ability to kinase-deficient mutants. *Proc Natl Acad Sci USA* **90:** 1518–1522.

Wu, J., Li, J., Li, G., Long, D.G., and Weis, R.M. (1996) The receptor binding site for the methyltransferase of bacterial chemotaxis is distinct from the sites of methylation. *Biochemistry* **35:** 4984–4993.

Wu, K., Walukietwicz, H.E., Glekas, G.D., Ordal, G.W., and Rao, C.V. (2011) Attractant binding induces distinct structural changes to the polar and lateral signaling clusters in *Bacillus subtilis* chemotaxis. *J Biol Chem* **286:** 2587–2595.

Zhao, J., and Parkinson, J.S. (2006a) Cysteine-scanning analysis of the chemoreceptor-coupling domain of the *Escherichia coli* chemotaxis signalling kinase CheA. *J Bacteriol* **188:** 4321–4330.

Zhao, J., and Parkinson, J.S. (2006b) Mutational analysis of the chemoreceptor-coupling domain of the *Escherichia coli* chemotaxis signaling kinase CheA. *J Bacteriol* **188:** 3299–3307.

Zheng, Q.S., Keszthelyi, B., Branlund, E., Lyle, J.M., Braunfeld, M.B., Sedat, J.W., and Agard, D.A. (2007) UCSF tomography: an integrated software suite for real-time electron microscopic tomographic data collection, alignment and reconstruction. *J Struct Biol* **157:** 138–147.

Zhou, Q., Ames, P., and Parkinson, J.S. (2009) Mutational analyses of HAMP helices suggest a dynamic bundle model of input–output signalling in chemoreceptors. *Mol Microbiol* **73:** 801–814.

Zhou, Q., Ames, P., and Parkinson, J.S. (2011) Biphasic control logic of HAMP signaling in the *Escherichia coli* serine chemoreceptor. *Mol Microbiol* **80:** 596–611.

Supporting information

Additional supporting information may be found in the online version of this article at the publisher's web-site.